Sequence-Dependent Bending of DNA Induced by Cisplatin: NMR Structures of an A·T-Rich 14-mer Duplex

John A. Parkinson,[a] Yu Chen,[a] Piedad del Socorro Murdoch,[a] Zijian Guo,[a] Susan J. Berners-Price,[b] Tom Brown,[c] and Peter J. Sadler*[a]

Abstract: The NMR solution structure of the A·T rich DNA 14-mer duplex d(ATACAT*GG*TACATA)·d(TATGTA*CC*ATGTAT) is reported. This is compared with the NMR structure of the same duplex intrastrand cross-linked at the d(G*pG*) site by *cis*-$\{Pt(NH_3)_2\}^{2+}$, derived from the anticancer drug cisplatin. The unmodified duplex has B-DNA geometry, but there is a large positive base-pair roll (roll angle $24\pm2^\circ$) at the T9–A10 step on the 3′ side of the central GG site. Platination of the DNA duplex causes the adjacent guanine bases to roll toward one another (roll angle $44\pm4^\circ$), leading to an overall helix bend of $52\pm9^\circ$. The platinum atom is displaced from the planes of the coordinated G7* and G8* by 0.8 Å and 0.3 Å, respectively. The minor groove opposite the platinum lesion is widened and flattened, with geometric parameters similar to those of A-form DNA. The unwinding of the helix at the platination site is 26°. Platination causes the DNA duplex to bend toward the 3′-end (with respect to the G*G* strand), in contrast to G·C-rich structures reported previously, which bend toward the 5′-end. This difference can be attributed to the predisposition of the A·T-rich duplex toward bending in this region. Protein recognition of bent platinated G*G* lesions may therefore exhibit a strong dependence on the local DNA structure.

Keywords: antitumor agents · bioinorganic chemistry · DNA structures · NMR spectroscopy · platinum

Introduction

The complex *cis*-$[PtCl_2(NH_3)_2]$, "cisplatin", is a widely used antitumor drug.[1] Its antitumor activity is believed to result from the strong bonding of the platinum to DNA, the local structure of which is subsequently modified in such a way that apoptosis is induced.[2] Cisplatin is known to form many kinds of DNA adducts. These include the major d(G*pG*) (70%), in which * indicates a platinated base, and d(A*pG*) (15%) 1,2-intrastrand cross-links, in which platinum binds through the purine N7 atoms. Other minor adducts include 1,3-intrastrand and interstrand cross-links.[1] The presence of these DNA cross-links in cisplatin-treated cancer patients correlates with positive responses to treatment with the drug.[3] Such lesions have deleterious effects on DNA replication and transcription[4] and cause mutations.[5] Proteins that contain one or more high-mobility-group (HMG) domains recognize and bind to intrastrand *cis*-$[Pt(NH_3)_2$-{d(G*pG*)}] and *cis*-$[Pt(NH_3)_2${d(A*pG*)}] adducts.[6–8] The shielding of excision–repair caused by the binding of HMG proteins to DNA has been confirmed by in vitro and in vivo experiments.[9, 10] Such biological effects are clearly correlated with the structures of the cisplatin-DNA adducts, and an understanding of the detailed structures of these DNA duplex adducts is therefore essential.

Several studies of structural distortions in cisplatin-DNA adducts have been reported. The X-ray crystal structure of *cis*-$[Pt(NH_3)_2$-{d[pG*pG*-N7(1),N7(2)]}] shows that cisplatin forms bidentate adducts, with the two adjacent guanines linked in a "head-to-head" configuration.[11] The dihedral angle between the two bases in this structure ranges from 72° to 82°. The 5′-G* deoxyribose sugar ring adopts the C3′-*endo* (N-type) conformation normally associated with A-DNA, whereas the 3′-G* sugar ring adopts the C2′-*endo* (S-type) pucker, which is more typical of B-DNA. In the 2.6 Å X-ray crystal structure of the dodecamer duplex d(5′-CCTCTG*G*TCTC C-3′)·d(5′-GGAGACCAGAGG-3′) (**IV***, Table 1),[12, 13] two independent molecules are observed with overall bends of 39°

[a] Prof. Dr. P. J. Sadler, Dr. Y. Chen, Dr. J. A. Parkinson, Dr. P. del Socorro Murdoch, Dr. Z. Guo
Department of Chemistry, University of Edinburgh
Edinburgh EH9 3JJ (UK)
Fax: (+44) 131-650-6452
E-mail: p.j.sadler@ed.ac.uk

[b] Dr. S. J. Berners-Price
School of Science, Griffith University
Brisbane (Australia)

[c] Prof. Dr. T. Brown
Biological and Medical Sciences Building
University of Southampton, Boldrewood Bassett Crescent East
Southampton, SO16 7PX (UK)

Supporting information for this article is available on the WWW under http://www.wiley-vch.de/home/chemistry/ or from the author.

0947-6539/00/0619-3636 $ 17.50+.50/0 *Chem. Eur. J.* **2000**, *6*, No. 19

Table 1. Major structural parameters of G*G* platinated DNA structures and the unplatinated 14-mer duplex **III**.

Sequence	**5′-ATACATGGTACATA 3′-TATGTACCATGTAT (14-mer)**		**5′-CCTCTGGTCTCC 3′-GGAGACCAGAGG (12-mer)**[a]		**5′-CTCTCGGTCTC 3′-GAGAGCCAGAG (11-mer)**
structure	**III**	**III***	$\mathbf{IV}_a^*$[12]	$\mathbf{IV}_b^*$[16]	**V***[17]
method	NMR	NMR[b]	X-ray[b]	NMR[b]	NMR[c]
DNA form	B	primarily B	A/B junction	primarily B	primarily B
minor groove width [Å]	5.2 ± 1.8[d]	8.0–11.0[e]	9.5–11.0[e]	9.4–12.5[e]	9.0–12.0[e]
depth [Å]	4.7 ± 0.7	1.3 ± 1.0	3.0	1.4	2.1
P-P distance [Å]	7.0	6.3	5.5	6.9	6.8
roll at G*G* bases [°]	-6 ± 3	44 ± 4	26	49	59
Pt atom displacement [Å][f]	–	0.8, 5′; 0.3, 3′	1.3, 5′; 0.8, 3′	0.8, 5′; 0.8, 3′	0.5, 5′; 0.65, 3′
average helix twist [°]	37.5 ± 0.2	29 ± 0.5	32	25	26
DNA bend [°]	18 ± 6	52 ± 9	39 and 55[g]	78	~81

[a] The same platinated DNA 12-mer duplex was studied by X-ray ($\mathbf{IV}_a^*$) and NMR ($\mathbf{IV}_b^*$). [b] *cis*-$\{Pt(NH_3)_2\}^{2+}$ adduct. [c] Spin-labeled adduct *cis*-$\{Pt(NH_3)$(4-amino-TEMPO)$\}^{2+}$ was used in this study. [d] Minor groove width measured as an average for the entire sequence. [e] Range in minor groove width at the platinum binding site only. [f] From plane of coordinated G. [g] Two independent molecules.

and 55°. Bending is largely the result of an inter-base roll of 26° at the G*G* site. This causes the minor groove to widen and flatten at this point and the major groove to become more compact. The Pt atom is displaced from the plane of each guanine base by approximately 1 Å.

The determination of NMR solution structures of platinated DNA duplexes allows assessment to be made of the effects of crystal-packing forces. Early NMR studies of the solution structures of cisplatin-induced 1,2-intrastrand cross-links in double-stranded DNA used the decanucleotide duplex d(GCCG*G*ATCGC)·d(GCGATCCGGC).[14] This duplex is kinked by 60° toward the major groove at the platinum coordination site and unwound by 12–19°. Models also suggest that the cytosine complementary to 5′-G* is rather mobile. The NMR solution structure of the platinated octamer duplex d(CCTG*G*TCC)·d(GGACCAGG)[15] shows that it is unwound by approximately 21° and kinked by approximately 58° toward the major groove at the G*G* site, the minor groove being significantly widened and flattened at the platination site. The NMR solution structure of the platinated dodecamer duplex ($\mathbf{IV}_b^*$, Table 1), with the same DNA sequence as that used in a previous X-ray study ($\mathbf{IV}_a^*$), has also been reported.[16] Although the unwinding and flattening of the minor groove opposite the platination site is similar in both the solution and crystal structures, the overall helical bend (78°) and the roll between adjacent guanine bases (49°) is more exaggerated in the solution structure compared with the X-ray crystal structure. The unwinding of the helix at the site of platination is 25° and the Pt atom is displaced from each base plane by ~0.8 Å. These differences between helix deformations in solution and crystal structures may be attributable to crystal packing interactions. The NMR solution structure of the G*G*-platinated adduct of the nitroxide spin-labeled complex *cis*-$\{Pt(NH_3)$(4-amino-TEMPO)$\}^{2+}$ with the undecamer d(CTCTCG*G*TCTC)·d(GAGACCGAGAG)[17] has been determined from conventional NOE studies of the reduced, diamagnetic undecamer, supplemented with long-range (10–20 Å) electron–proton restraints from the paramagnetic duplex. The additional restraints did not affect the local geometry of the adduct, only the global structure.

In this report, the solution structures of both free and GG-platinated DNA 14-mer duplex d(ATACATGGTACATA)·d(TATGTACCATGTAT) have been determined by NMR spectroscopy and restrained molecular dynamics (rMD) simulations. This duplex possesses over one turn of helix and appears to be the longest used to date in detailed solution NMR structural studies of DNA platination, as well as being the most A·T rich.

5′-d(A_1 T_2 A_3 C_4 A_5 T_6 G_7 G_8 T_9 A_{10} C_{11} A_{12} T_{13} A_{14}) **I**

3′-d(T_{28} A_{27} T_{26} G_{25} T_{24} A_{23} C_{22} C_{21} A_{20} T_{19} G_{18} T_{17} A_{16} T_{15}) **II**

I + II = III

Results

NMR data assignment: The platinated single strand **I*** purified by HPLC and platinated duplex **III*** each gave rise to two $^1H/^{15}N$ cross-peaks in two-dimensional [^1H,^{15}N] HSQC NMR spectra (Figure S1 in the supporting information): δ $^1H/^{15}N$(**I***) = 4.58/−65.19, 4.51/−66.49; δ $^1H/^{15}N$(**III***) = 4.43/−70.45, 4.20/−70.26, in agreement with previous NMR data for this oligonucleotide.[18]

^1H NMR resonances for **III** and **III***, were assigned from 150 and 300 ms two-dimensional NOESY NMR data sets by using established methods.[19, 20] Correlations (NOEs) between aromatic and H1′ proton resonances are shown in the supporting information for **III*** (Figure S2 in the supporting information) as are similar assignment data for the unmodified duplex, **III** (Figure S3 in the supporting information). Complete sets of sequential NOEs between *n*H8/H6 to *n*H1′ and between *n*H1′ to (*n*+1)H8/H6 for separate strands of each DNA duplex **III** and **III*** were traced. The H8 resonances of the two platinated bases G7* ($\delta = 8.64$) and G8* ($\delta = 8.08$) of **III*** were shifted to high frequency relative to **III** (G7, $\delta = 7.75$; G8 $\delta = 7.56$). Strong NOEs were observed between G7* H8 and G8* H8 of **III*** consistent with previous reports on G*G* duplexes,[15, 16] but, in contrast, were not observed for **III**. NOESY NMR spectra acquired at different sample temperatures were used to clarify assignments for some of the overlapped cross-peaks in both cases.

Analogous NOESY assignment pathways between base and sugar protons were used to assign H3′, H2′, and H2″ resonances for both **III** and **III***. A significant, low-frequency shift was noted for the T6 H2′ resonance in the platinated duplex **III*** ($\delta = 1.37$ in **III*** compared with $\delta = 1.92$ in **III**). A combination of two-dimensional NOESY and DQF-COSY NMR data sets was used to complete and confirm the

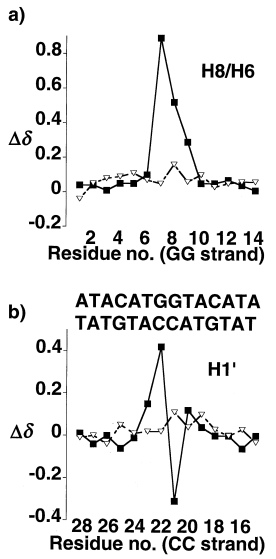

Figure 1. Chemical-shift differences for NMR resonances of platinated and unplatinated DNA duplexes. Chemical shift differences, $\Delta\delta$, measured as (δ**III*** - δ**III**) for a) aromatic and b) H1′ resonances. Shift changes are indicated for the platinated GG strand (■) and for the complementary CC strand (▽).

assignments for most of the sugar proton resonances including H4′ and some of the H5′/H5″ signals. Table S1 and S2 in the supporting information detail ^{1}H resonance assignments for **III*** and **III**, respectively.

Structural changes in DNA induced by ligand binding can be revealed by differences in chemical shifts ($\Delta\delta$) between free and ligand-bound duplexes.[21] Clear differences are revealed (Figure 1) for aromatic and H1′ chemical shifts upon platination of **III** to give **III***. Large deshielding perturbations are observed for the central G7 and G8 aromatic proton resonances, the effect also extending to the neighboring T9 base. The complementary strand is relatively unaffected in this respect. The largest changes in H1′ chemical shifts occur for the G7* and G8* residues, but, in these cases, the shift changes are of opposite sign: G7* H1′ is deshielded whereas G8* H1′ is significantly shielded upon platination. Each of these changes is indicative of a local change in geometry which occurs in the DNA when it becomes platinated.

Assignments of exchangeable protons were made by analysis of the 300 ms two-dimensional NOESY data sets acquired at 278 K on samples dissolved in 90 % H_2O/10 % D_2O. Inter-base-pair NOEs involving neighboring residues were used to assign imino proton resonances. The assignment pathway for **III*** (Figure S4 in the supporting information) was interrupted only at the G7* site, although imino proton resonances for the base-pairs A1·T28, T2·A27, T13·A16, and A14·T15 at the 5′ and 3′ ends were absent, as anticipated. The G7* imino proton resonance was assigned by comparing one-dimensional ^{1}H NMR data at different temperatures (Figure S5 in the supporting information). By lowering the temperature, an imino proton NMR signal at $\delta = 13.49$ gradually increased in intensity and became clearly visible at 278 K. No NOE was observed between this proton and other imino protons, but inter-base NOEs between G7* imino- and C22 amino protons were retained, although weaker than the equivalent G8* imino to C21 amino proton NOEs. The imino proton resonances of G7* ($\delta = 13.49$) and G8* ($\delta = 13.06$) of **III*** were shifted to high-frequency (deshielded) realative to those of G7 ($\delta = 12.55$) and G8 ($\delta = 12.67$) for **III**, a similar behavior to the G7* and G8* aromatic proton resonances. Significant deshielding was also observed for the adjacent base-pair imino proton resonances: T6 H3 of **III*** ($\delta = 13.96$) compared with T6 H3 of **III** ($\delta = 13.40$); T9 H3 of **III*** ($\delta = 13.80$) compared with T9 H3 of **III** ($\delta = 13.33$). These are also a reflection of changes that occur in the local geometry of the DNA structure, although for G7* and G8* the deshielding observed at N1 is likely to be influenced by electronic effects caused by bound Pt.

Analysis of sugar ring conformations: The intra-nucleotide NOE between the H8 and H3′ protons of the G7* residue was strong relative to the same interaction for either G8* of **III*** or the G7/G8 residues in **III**. The binding of cisplatin to DNA has been shown to alter the 5′-G deoxyribose ring conformation relative to that of the 3′-G residue.[15–17] In the present case, the NOE information indicated that G7* and G8* sugar puckers in **III*** were of different types. DQF-COSY NMR data confirmed this difference. Strong NOEs were observed between G7* H1′ and G7* H2′ and between G7* H1′ and G7* H2″. However, no DQF-COSY cross-peak was observed between G7* H1′ and G7* H2′, and the G7* H1′ to H2″ cross-peaks differed significantly in appearance compared with the H1′ to H2″ DQF-COSY cross-peaks for all other residues. The programs SPHINX and LINSHA were used to simulate the DQF-COSY cross-peak patterns. These confirmed that the G7* sugar pucker is C3′-*endo* (N-type), a conformation usually associated with A-type structures. The remaining sugar puckers were of the C2′-*endo* (S-type) or closely related C3′-*exo* type and are characteristic of B-DNA structures (Figure S6 in the supporting information; see also note added in proof).

Determination of the structures of platinated duplex III* and unmodified duplex III: The two-dimensional NOESY NMR data sets were used for quantitation of NOEs and structure calculations. Statistical data for the restraints used in the calculation of each NMR structure are shown in Table 2. The

Table 2. Statistical data for the final sets of restraints used in the NMR structure calculations for the 14-mer DNA duplexes **III** and **III***

Restraint	Structure	
	III	**III***
NOE restraint		
quantitative (total)	421	574
intra-residue	277	367
inter-residue	144	207
qualitative	24	49
Watson–Crick distance restraint	32	32
Watson–Crick flat angle restraint	32	32
deoxyribose torsion angle restraint	140	140
total	649	827
average restraints per residue	23	30

difference between the average number of restraints per residue for **III** and **III*** is in part a reflection of the increased dispersion in the NMR data for **III***, an effect brought about by drug binding at G*G* (Figure 1). The data were generally of high quality, resulting in a large number of inter-proton NOE assignments. Structure calculations were based on three rounds of MARDIGRAS calculations, followed by rMD runs for both **III** and **III***. The average structure from the last 3 ps of one rMD run served as the starting model for the next series of distance calculations. The initial structure calculations for **III*** were carried out in the absence of platinum. In this way only the distance and angle restraints for the DNA

0947-6539/00/0619-3638 $ 17.50+.50/0 *Chem. Eur. J.* **2000**, *6*, No. 19

influenced the structure. After the first round of calculations for **III*** from either **A-** or **B-**DNA starting models, the G*G* binding site clearly adopted a conformation which allowed $\{Pt(NH_3)_2\}^{2+}$ to be docked without significant disruption to the surrounding DNA structure. Further calculations of this structure proceeded with the bound complex. The program CORMA was used for NMR data simulation by back-calculation from A- and B-DNA and from the final structures **III** and **III*** (Figure S7 in the supporting information). Crystallographic, R, and sixth root, R^x, factors from these calculations are shown in Table 3. The final structures fit the experimental data better than the idealized starting models as shown by an overall reduction in the size of the factors and in the extent of NOE violations (Δd_{av}), calculated as the average distance violation of all upper and lower distance violations relative to those of the starting models.

Structure of the platinated 14-mer DNA duplex III*: All of the NMR data acquired on **III*** suggest that, under the conditions used, the duplex exists predominantly as a single structure in solution on the NMR timescale. The set of sequential NOEs between the base aromatic and sugar H1′, H2′/H2″, and H3′ proton resonances is consistent with a stable, right-handed, double-helical structure, with the majority of bases orientated in the *anti*-configuration.

Starting from either A- or B-form DNA models, the structures converged to give a final calculated structure for **III***, which was considerably distorted compared with either canonical A- or B-DNA. The family of ten low-energy calculated structures for **III***, shown in Figure 2, has a pair-wise, all-atom root-mean-square deviation (rmsd) of 1.2 ± 0.2 Å. This is in contrast to the pair-wise all-atom rmsd of 6.7 Å between the A- and B-DNA starting models. A single coordinate set for **III*** was calculated from an average of these structures and used for CORMA and CURVES calculations.

Space-filling and line representations of the DNA structure **III*** are shown in the supporting information in Figures S8B and S9B, respectively. Despite its considerable bend, the structure can be classed as B-form DNA, according to i) the type of pucker adopted by the sugar rings (predominantly C2′-*endo*, or the related C3′-*exo* conformations), and ii) the phosphate–phosphate distances across the minor groove (average = 6.28 Å). The G7* deoxyribose ring adopts a C3′-*endo* sugar conformation, consistent with both NOESY and with simulated and experimental DQF-COSY NMR data (Figure S6 in the supporting information).

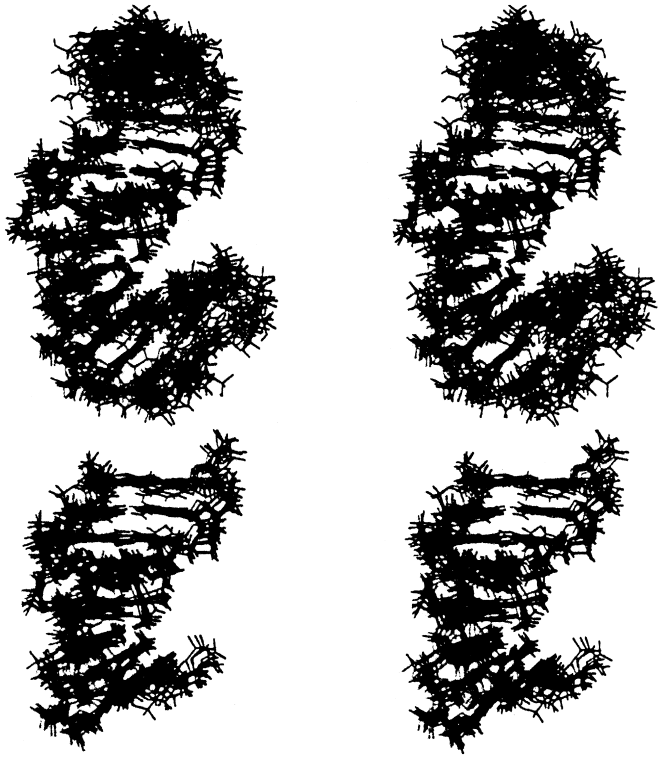

Figure 2. NMR solution structure of the platinated 14-mer DNA duplex, **III***. Relaxed eye stereo images of ten complete structures of **III*** (top, averaged pair-wise all-atom rmsd = 1.2 ± 0.2 Å) and a view (bottom) of the central eight base pair region $C_4A_5T_6G^*_7G^*_8T_9A_{10}C_{11}\cdot G_{18}T_{19}A_{20}C_{21}$-$C_{22}A_{23}T_{24}G_{25}$ (averaged pair-wise all-atom rmsd = 1.07 ± 0.1 Å). The duplex is unwound and the base pairs are destacked at the G*G* site. Bending of the helix axis into the major groove is apparent in the central region of the duplex.

The overlay of the family of structures shown in Figure 2 is tighter toward the center of the duplex than at either end. This is a consequence of the limitations in the extent of NOE data, which, for DNA, does not include long-range distance constraints. It has been noted previously that convergence can be worse for terminal than for internal residues in DNA structures determined by NMR spectroscopy.[26] This is a reflection of experimental bounds for terminal residues being inconsistent with a single structure, and is usually attributed to fraying at the duplex ends. In the central region, the binding of *cis*-$\{Pt(NH_3)_2\}^{2+}$ to the N7 atoms of the adjacent guanine bases G7* and G8* causes a roll of 44 ± 4° toward the major

Table 3. Crystallographic (R) and sixth-root (R^x) factors and residual NOE violation factors (Δd_{av}) for the A- and B-DNA starting models and the final NMR structures **III** (unmodified 14-mer DNA duplex) and **III*** (platinated 14-mer DNA duplex) calculated by using the program CORMA.

Factor						**Platinated structure**			
	A-DNA			B-DNA			**III***		
NOE	intra[a]	inter[b]	global[c]	intra	inter	global	intra	inter	global
R	0.535	0.696	0.571	0.431	0.597	0.475	0.359	0.491	**0.399**
R^x	0.125	0.150	0.132	0.101	0.121	0.107	0.069	0.087	**0.075**
Δd_{av} (Å)		0.69			0.66			**0.34**	
						Unmodified structure			
	A-DNA			B-DNA			**III**		
NOE	intra	inter	global	intra	inter	global	intra	inter	global
R	0.845	0.437	1.000	0.734	0.873	0.770	0.730	0.870	**0.726**
R^x	0.201	0.092	0.198	0.290	0.201	0.260	0.300	0.195	**0.263**
Δd_{av} (Å)		0.37			0.31			**0.27**	

[a] Intra for which only intra-residue NOEs are considered. [b] Inter for which only inter-residue NOEs are considered. [c] Global for which all NOEs are considered.

  0947-6539/00/0619-3639 $ 17.50+.50/0

groove; this results in a calculated global bend of the duplex of $52 \pm 9^\circ$. The bending point of the helix axis is located at T9, on the 3′ side of G7*G8*, rather than directly at the platinated G7*G8* base step. The roll and the geometric distortion at the G7*G8* base step reflect the NMR data, which show an intense cross-peak between G7* H8 and G8* H8 in both experimental and back-calculated NOESY data sets (Figure S7 in the supporting information).

A stereo view of the platinated G7*G8* site of **III*** is shown in Figure 3. The G7* and G8* bases are coordinated to the Pt center in a head-to-head fashion. Hydrogen bonding between the 5′-G7*·C22 base pair is severely affected, consistent with weak NOEs observed between the iminoproton of G7* (H1) and the amino protons (H4(1)/ H4(2)) of the partnering base, C22. The Pt atom is displaced from the planes of the coordinated guanine bases by 0.8 Å for G7* and 0.3 Å for G8*. The purine ring of G7* does not stack on either the G8* or the T6 bases, but the corresponding bases of the complementary strand are still stacked. The distortions caused by platination also include a large positive stretch and buckle at the G7*·C22 base pair and significant opening and stagger at G8*·C21.

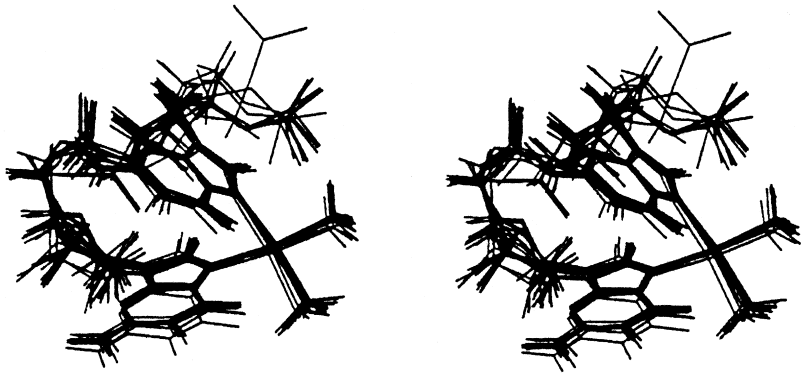

Figure 3. NMR solution structure of the G*G* platination site of **III***. Relaxed eye stereo image of **III*** as an overlay of ten structures.

The resonances of both G7* H8 ($\delta = 8.64$) and G8* H8 ($\delta = 8.08$) are shifted to high frequency relative to G7 H8 ($\delta = 7.75$) and G8 ($\delta = 7.56$) in the unmodified duplex. The observation is consistent with the bases being in an *R* conformation, which is usually observed for G*G* intrastrand platinated DNA duplexes.[22] The T6 deoxyribose sugar ring is also affected by the platinum cross-link at the G7*G8* site, which induces characteristic chemical shift variations for T6 H1′ (from $\delta =$ 5.71 to 5.86) and H2′ (from $\delta = 1.92$ to 1.37) relative to **III**. Similar shifts for the sugar H1′ and H2′ resonances of T residues, 5′ to a G*G* platination site, have been reported previously.[15, 16, 23] The T6 H2′ proton is therefore located in the shielding cone of the G7* base, which is consistent with our model (see also note added in proof).

Compared with B-DNA, the minor groove opposite the site of platination in **III*** is widened and more shallow. Canonical B-DNA has an average minor groove width of 5.87 Å and a depth of 4.63 Å.[24] The minor groove of **III*** is opened to between 8 and 11 Å over the region G7* to A10 and has a depth ranging from 3.9 to 1.3 Å. The biggest groove width and the shallowest groove depth coincide with the T9 – A10 step. The variation in minor-groove width with base-pair step is depicted in Figure 4. The platinated DNA structure shows significant unwinding with a twist of approximately 29°. The structural data for the final platinated DNA structure are detailed in Table 1 and compared with published data on related platinated duplexes.

Structure of the unmodified 14-mer DNA duplex III: The structure of the unmodified duplex **III** was determined so that the effects of platination could be assessed directly. Structure determination was carried out as described for **III***. By inspection, the data were consistent with right-handed B-DNA geometry. Convergence from A- and B-DNA starting models was achieved in three rounds of calculations. With fewer constraints per residue, the overlay of final structures was generally poorer compared with **III***. The average pair-wise all-atom rmsd of 2.4 Å for ten low-energy structures is larger due to poor fitting at the ends of the structures. However, the central six base-pair region shows a good fit against the mean (six base-pair all-atom rmsd = 0.77 Å for ten structures). An overlay of three structures from these calculations is shown in Figure 5. Two of the structures derive from A- and B-DNA starting models, each of which is the average of a family of five structures from the final round of calculations. The third structure is the mean of the previous two. The average pair-wise all-atom rmsd over the whole structure for these average models (1.13 Å) coincides with the reduction in NOE violations, (Δd_{av}), and *R* and sixth-root R^x factors (Table 3). The geometry of the structure, evaluated by using the program CURVES from a set of averaged coordinates (Figures S8A and S9A in the supporting information), and

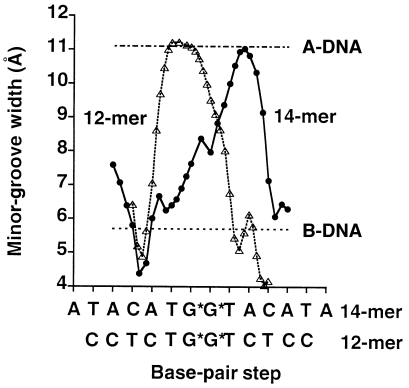

Figure 4. Minor groove width of **III***. Variation in minor groove width (Å) with base-pair step for the 14-mer **III*** (●) compared with the G·C rich 12-mer $\mathbf{IV}_b^*$[16] (△). The minor groove widths of canonical A- and B-form DNA are plotted as horizontal lines for comparison.

0947-6539/00/0619-3640 $ 17.50+.50/0 *Chem. Eur. J.* **2000**, *6*, No. 19

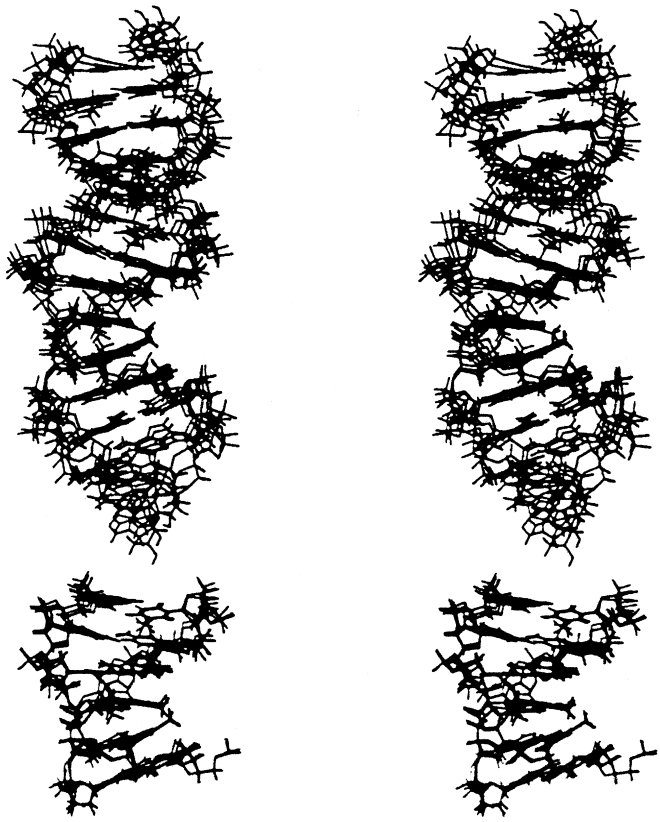

Figure 5. NMR solution structure of **III**. Relaxed eye stereo images as an overlay of three structures of **III** (top), two of which are the average of five structures from each of the A- and B-DNA based structure calculations, the third being the mean of these two (averaged pair-wise all atom rmsd = 1.13 Å). A view of the central six base pair region (bottom) $T_6G^*_7G^*_8T_9A_{10}$-$C_{11}\cdot G_{18}T_{19}A_{20}C_{21}C_{22}A_{23}$ (averaged pair-wise heavy atom rmsd = 1.06 ± 0.07 Å) shows the nature of the kink at the T9–A10 step.

the average minor groove width (5.2 ± 1.8 Å) and depth (4.8 ± 0.7 Å) are consistent with a B-DNA duplex. The large positive base-pair roll ($\rho = 24 \pm 2^\circ$), which occurs at the T9–A10 step, is much more significant than that for any of the other base-pair steps (Figure S10 in the supporting information) and effectively kinks the DNA. The local dimensions of the minor groove at the T9–A10 step describe this kink (width: 8.5 ± 0.1 Å; depth: 3.7 ± 0.4 Å; global axis curvature angle: 12.75°). Overall the duplex is bent by 18 ± 6°. Further structural details for **III** are given in Table 1.

Discussion

Although the major and minor grooves provide the topology of duplex DNA, subtle, sequence-dependent structural variations can occur; these include relatively gross changes in bending and groove widths.[25] The DNA sequence d(ATACATGGTACATA)·d(TATGTACCATGTAT) (**III**), is A·T rich (71%) compared with the DNA sequences (A·T content: 25–37%) used previously in the structural studies of intrastrand DNA platination.[12, 15–17] In previous studies, the GG strand has been pyrimidine rich (ca 82%) whereas in **III** the purines and pyrimidines are more evenly distributed between the two strands, an alternating purine-pyrimidine sequence occurring for all except the central base pairs. Such a difference in sequence is very significant: neighboring base pairs are known to influence one another in terms of their relative orientation, reflected in base-pair roll angles.[26, 28] This characteristic feature of neighboring base pairs has a dramatic effect on the overall structure of a DNA sequence. For example, pyrimidine-purine sequences have a tendency toward positive roll bending, whereas an A-tract (four successive As or Ts) behaves more as a rigid rod.[28]

Previously, we have used **III** in kinetic studies of DNA platination and observed a remarkably long-lived 5′-G monofunctional adduct during the course of the formation of the G*pG* bifunctional adducts.[27] The present study reveals that the NMR solution structure of **III*** is distorted in a generally similar way to previously reported structures of G*pG* intrastrand-platinated DNA duplexes.[15–17] The bending angle (52 ± 9°) of **III*** is less than those of the reported solution structures $\mathbf{IV}^*_b$ (78°)[16] and **V*** (81°),[17] but close to that of a reported 8-mer (58°)[15] and to those found in the X-ray crystal structure of the 12-mer, $\mathbf{IV}^*_a$ (39° and 55°), Table 1.[13] The overall shape of **III*** is very similar to that in the reported X-ray crystal structure $\mathbf{IV}^*_a$ and the NMR solution structure **V*** determined by combining long-range electron–proton and short-range inter-proton distance restraints, Table 1.

The major structural difference between **III*** and structures, $\mathbf{IV}^*_a$, $\mathbf{IV}^*_b$ and **V*** (Table 1) is the bending position of the duplex. For **III***, both the widest and the shallowest parts of the minor groove occur at the T9–A10 step, with the result that the 3′ side of **III*** (with respect to the G*G* strand) is much more bent toward the major groove than the 5′ side. This contrasts sharply with structures $\mathbf{IV}^*_a$, $\mathbf{IV}^*_b$ and **V***[13, 16, 17] in which the side 5′ to G*G* is bent more toward the major groove and contains the widest minor groove. These structural differences suggest that platinum-induced distortions of DNA are also related to sequence-dependent structural variations of the DNA itself.

The base sequence of **III** has only one G·C base pair on either side of the G7*G8* sequence, separated by two A·T base pairs. The data from CURVES show that both the G7*-G8* and T9–A10 base steps have large positive rolls. The former is due to the binding of $\{Pt(NH_3)_2\}^{2+}$, while the roll at T9–A10 is a feature typical of pyrimidine-purine steps including C-A (= T-G), T-A, or less frequently C-G steps.[26, 28] The presence of the extra T-A step 3′ to the G7*-G8* site of **III***, which is not found with duplexes **IV*** or **V***, probably accounts for the switch in the bending point from the 5′ to the 3′ side of G*G*. A large positive base-pair roll (24 ± 2°) at the T9–A10 step also occurs in the unmodified duplex **III**, consistent with other DNA structures,[26, 28] thereby altering the DNA minor groove geometry at this point and bending the DNA. These changes coincide with the shallowest and widest part of the minor groove in the structure of **III***; this implies that the sequence itself is predisposed to bending at a position 3′ to the G*G* site.

DNA bending is known to be sequence-dependent.[28] For example, distortions of DNA induced by mono-functional binding of $\{Pt(dien)\}^{2+}$ depend on the sequence[29] and, remarkably, the most pronounced effects are observed when the adduct is flanked by single pyrimidines on both 3′ and 5′

sides. Although pyrimidine-purine sequences are disposed toward positive roll bending, the effect depends on the environment. Bending occurs only when a suitable stress is applied. Many examples exist in which C-A or T-G steps result in no overall DNA bending.[28]

In the current example, there are two hinges on either side of the G7*-G8* platination site of **III***, that is, to the 5′ side (T6-G7*) and to the 3′ side (T9 – A10), both of which could cause roll bending. For **III***, this effect is greatest at the G8*-T9 – A10 steps, which causes the 3′ side of the DNA to bend toward the major groove. Each reported Pt-DNA structure $\mathbf{IV}_a^*$, $\mathbf{IV}_b^*$ and **V*** has at most only one pyrimidine-purine step on either side of the G*G* site. In these cases, the positive roll at both the T-G* (or C-G*) and the G*-G* steps causes the 5′-side of the DNA duplex to bend toward the major groove, the minor groove being opened at these points.

The imino proton resonance of the 5′-G* residue has been observed in only a few reported NMR structural studies of intrastrand G*G* cross-linked DNA duplexes at low temperature.[52] This can be explained by the distortion of the 5′ G*·C base pair by the G*-G* bischelate. In previous reports, the mobility of the cytosine complementary to 5′-G* results in fast exchange of the 5′-G* imino (H1) proton with the solvent.[14] In contrast, for **III*** the intensity of the 5′-G7* imino proton resonance was relatively strong at low temperature and showed clear NOE connectivities to the partnering C22 amino (H4(1) and H4(2)) protons. The Watson – Crick base-pair between G7* and C22 in **III*** therefore remains relatively intact. This observation is consistent with the calculated structure of **III*** in which the helix bend occurs at a position remote from this point (at the T9 – A10 base step on the 3′-flanking side of G7*-G8*). This causes the hydrogen bonding between G7* and C22 to be less affected than in previous structures,[15–17] which have the bending point on the 5′ side of G*G*. The absence of NOE connectivities between the imino proton of G7* and the nearby T6 and G8* residues of **III*** suggest that the base stacking is disordered at the G7*G8* site.

In a related study, we have examined, by ^{1}H NMR spectroscopy, the adduct formed between the new anticancer drug *cis*-[$PtCl_2(NH_3)$(2-picoline)] (ZD0473) and the 14-mer DNA duplex **III**.[30] The NOE data for protons around the platination site were fitted to a model based on the platinated duplex structure **III*** calculated in this work. It was possible to replace *cis*-$\{Pt(NH_3)_2\}^{2+}$ in **III*** by the fragment *cis*-$\{Pt(NH_3)$(2-picoline)$\}^{2+}$ from ZD0473[31] with little rearrangement of the duplex conformation, and to satisfy all of the NOE connectivities between the 2-picoline ligand and the nearby T6 and G7* protons.[30] The ring-current effect of the 2-methylpyridine ligand on the T6 H2′ resonance was readily accounted for by this model. This platination is highly stereoselective, the dominant conformer having the 2-picoline ligand oriented toward the 5′ end and the methyl substitiuent oriented toward the center of the major groove. However, similar attempts to dock *cis*-$\{Pt(NH_3)$(2-picoline)$\}^{2+}$ onto the previously reported structures of intrastrand G*G* platinated DNA duplexes $\mathbf{IV}_a^*$ and **V*** were unsuccessful, even though the central four base pairs, TG*G*T, are the same as those for **III***. The location of the bending sites in $\mathbf{IV}_a^*$ and **V*** on the 5′ side of the G*-G* site leads to unfavorable steric interactions between the 2-picoline ligand and the surrounding nucleotides. Therefore the local structural perturbations at intrastrand G*G* cross-links induced by *cis*-$\{Pt(NH_3)_2\}^{2+}$ or *cis*-$\{Pt(NH_3)$(2-picoline)$\}^{2+}$ may be similar or different depending on the flanking sequences. This may have implications for protein and enzyme recognition.

The recent X-ray crystal structure of HMG domain A protein bound to cisplatin-modified DNA[32] has shown that HMG1-A binds to the widened minor groove. Interestingly, protein binding in this complex takes place exclusively on the 3′ flanking side of the platinated strand through its concave surface.[32] However, the *protein* bend is not centered at the platination site, but is translocated by two base pairs to the 3′-side. The sequence of the Pt-DNA adduct is known to have a significant influence on the strength of such protein – DNA interactions. Both domains (A and B) of the HMG1 protein bind preferentially to DNA that has A/T sequences flanking G*G*, with slightly different base pair preferences.[33] HMG1-A binds much more tightly than HMG1-B, typically with a 10- to 100-fold lower K_d value. Flexible A·T base pairs flanking the platinum lesion would facilitate further bending of the DNA duplex caused by HMG protein binding. The tighter binding of HMG1-A is also accompanied by a much more distinct flanking sequence specificity, with the nucleotide on the 3′ side of G*G* determining the sequence specificity. The base-pair at the 3′ position to the lesion has been reported to be highly accessible within the minor groove.[12, 34, 35] Although the HMG domain proteins share a common ability to bend platinated DNA, specific contacts between the proteins and the platinated duplex are different.[36] Different binding affinities of the two domains in the full-length protein may implicate sequence-dependent bending characteristics for different DNA sequences.[37] Sequence-dependent bending of G*G* intrastrand cross-linked DNA may thus be important for recognition by DNA-binding proteins.

Conclusion

We have determined the NMR solution structures of an A·T-rich DNA 14-mer duplex **III** and the same duplex platinated with *cis*-$\{Pt(NH_3)_2\}^{2+}$ (**III***). Platination causes the DNA duplex to bend toward the major groove. The minor groove opposite the platination site is widened and flattened. The structure of **III*** is categorized as B-DNA, but differs significantly from reported G*G* platinated duplexes in the position of DNA bending. Duplex **III** is kinked on the 3′ side of the GG site and susceptibility to bending in this region may explain why the platinated duplex **III*** is much more bent toward the major groove on the 3′ side compared with previously reported platinated DNA structures, all of which are bent on the side 5′ to the G*G* site. Kinking of **III** results from a large base-pair roll at the T9 – A10 pyrimidine-purine step. Two major factors therefore determine the structure of **III***: induced roll bending at the G7*G8* platination site and the inherent roll bending at the T9 – A10 base-pair step. These findings may have important implications for protein recognition of platinated DNA and the design of sequence-specific DNA-binding drugs.

0947-6539/00/0619-3642 $ 17.50+.50/0 *Chem. Eur. J.* **2000**, *6*, No. 19

Experimental Section

Materials and sample preparation:[^{15}N]-Cisplatin (*cis*-[$PtCl_2(^{15}NH_3)_2$]) and [^{15}N]-diaqua-cisplatin (*cis*-[$Pt(^{15}NH_3)_2(H_2O)_2]^{2+}$) were prepared as previously described.[38, 39] The sodium salts of HPLC-purified oligonucleotides d(ATACATGGTACATA) and d(TATGTACCATGTAT) were supplied by Oswel (Southampton, U.K.).

Preparation of DNA duplex (III): D_2O (60 μL) and $NaClO_4$ (60 μL, 60 μmol) were added to aliquots of strand **I** (146.3 μL, 0.60 μmol) and strand **II** (389.2 μL, 0.60 μmol) in H_2O. The pH of the solution was adjusted to 7.00. The final concentration of duplex **III** was 0.9 mM. The sample was annealed by heating to 353 K for 2 min and slow cooling to ambient temperature.

Platination of I by *cis*-[$Pt(^{15}NH_3)_2(H_2O)_2]^{2+}$: D_2O (50 μL), $NaClO_4$ (50 μL, 50 μmol), H_2O (4.2 μL), and freshly prepared *cis*-[$Pt(^{15}NH_3)_2(H_2O)_2]^{2+}$ (100 μL, 1 μmol) were added to an aliquot of strand **I** (295.8 μL, 1 μmol). The solution was kept at 298 K in the dark. The reaction was monitored by both two dimensional HSQC NMR spectroscopy and HPLC by using a Nucleosil C_8 300 Å stainless steel column. After one week of incubation, the reaction was judged to be complete, yielding the platinated single-strand **I***.

HPLC purification of I*: Separation and purification of the cisplatin-DNA single strand adduct, **I***, was performed by using Biocad perfusion chromatography on a Poros RV Column (100 × 4.5 mm). The operating conditions were: mobile phase, 5 mM ammonium acetate, 50% acetonitrile (gradient: 5% acetonitrile for 5 min; from 5 min to 19 min 5% to 25%, from 19 min to 22 min 25%), flow rate 1 mL min^{-1}, 298 K. The DNA single strand and the platinated DNA adduct had retention times of 7.7 min and 14.9 min, respectively. The platinated adduct was collected and freeze-dried to remove volatile salts and its purity checked by both HPLC, one-dimensional ^{1}H- and two-dimensional [^{1}H,^{15}N] HSQC NMR spectroscopy.

Formation of platinated duplex III* from II and I*: Duplex **III*** (0.9 mM in 100 mM $NaClO_4$, 90% H_2O/10% D_2O, pH 6.2) was prepared by adding 1 mol equivalent of the complementary DNA strand, **II**, to the purified platinated DNA strand, **I***. Dioxane ($\delta = 3.767$, 25°C) was added as an internal ^{1}H NMR reference. The concentrations of the DNA single strands **I*** and **II** were measured by UV spectrometry (ε_{260} values strand **I***: 149 mM^{-1} cm^{-1}; strand **II**: 137.2 mM^{-1} cm^{-1}). The precise ratio of the two strands was also monitored by one-dimensional ^{1}H NMR spectroscopy. **III*** was annealed by heating briefly to 343 K followed by slow cooling to ambient temperature. The extent of duplex formation was verified by one-dimensional ^{1}H and two-dimensional [^{1}H, ^{15}N] HSQC NMR spectroscopy. **III*** was separately freeze-dried from 90% H_2O and dissolved in 99.9% D_2O for studies of non-exchangeable protons only.

NMR spectroscopy: NMR data were acquired on 500 MHz Bruker DMX and Varian Unity *plus* NMR spectrometers and on 600 MHz Varian Unity and Unity *INOVA* NMR spectrometers by using *z*-field gradient, triple resonance probe-heads. One-dimensional ^{1}H NMR spectra were typically acquired at 500 MHz with 128 transients into 32768 data points over a spectral width of 10.5 kHz by using a double-pulsed-field-gradient-spin-echo (DPFGSE) pulse sequence.[40] Two-dimensional [^{1}H,^{15}N] HSQC NMR data sets were acquired and processed according to previously reported methods.[39] Two-dimensional NOESY and DQF-COSY NMR spectra were acquired at temperatures of 278 and 298 K. Two-dimensional NOESY data sets were acquired with 48 transients over a ^{1}H spectral width of 21 ppm (10.5 kHz) into 4096 data points for each of 512 t_1 increments (TPPI) using a mixing time of 150 ms. The solvent signal was suppressed by using a DPFGSE routine.[40] High resolution two-dimensional NOESY data sets were acquired on samples in 99.9% D_2O (278 K at 600 MHz) over a ^{1}H spectral width of 9 ppm (5.4 kHz) into 4096 data points for each of 2 × 512 t_1 (States)[41] increments with mixing times of 150 and 300 ms and a recycle delay of 3.5 s. Two-dimensional DQF-COSY data sets were acquired with 96 transients for each of 2 × 512 t_1 (States) increments over a spectral width of 10 ppm. Presaturation was used to eliminate the solvent signal in both cases. Raw data were imported into Xwinnmr version 2.0 (Bruker UK). Processed data were exported into the TRIAD NMR module of Sybyl (version 6.3, Tripos Inc.) for data reduction.

pH Measurements: pH Measurements were made by using a Corning 145 pH meter equipped with an Aldrich micro-combination electrode calibrated with Aldrich buffer solutions of pH 4, 7, and 10. Values of pH were adjusted with 1M $HClO_4$ or NaOH as appropriate.

NMR data assignment strategy: NOESY data were assigned for both free- and platinated-DNA duplexes, **III** and **III***, by using established assignment strategies[19, 20] for right-handed B-form DNA. DQF-COSY data were used to confirm the assignments of H2′ and H2″ resonances and to provide data on sugar ring conformations.

Modeling restraints: Quantitative inter-proton distance restraints for non-labile protons were calculated by using an iterative relaxation matrix approach with the program MARDIGRAS.[42, 43] Averaged cross-peak volume integrals from two-dimensional NOESY NMR data acquired for samples of **III** or **III*** in D_2O were used in relaxation matrix calculations starting from both canonical A- and B-DNA models. Distance ranges were calculated by averaging over all upper distance bounds to yield a set of averaged upper bounds, and over all lower distance bounds to yield a set of averaged lower bounds. Qualitative distance restraints, incorporated for all NOEs associated with exchangeable protons, were based on an assessment of strong, medium, or weak signal intensitites as distance bounds in the ranges 2.5 to 5.0 Å, 3.5 to 5.0 Å, and 4.5 to 5.0 Å, respectively. Watson–Crick hydrogen-bond-length and flat-angle restraints were introduced to encourage base-pairing and to prevent the two strands of the duplexes from flying apart when the temperature was raised during simulations. Such restraints are commonly used in DNA structure determinations from NMR data.[26, 44] Hydrogen-bond-lengths and flat angles were defined according to crystallographic measurements.[45] Hydrogen-bond-length restraints were set to 10 kcal mol^{-1} Å^{-2} and flat-angle restraints (between the three atoms forming each hydrogen bond) were set to 0.01 kcal mol^{-1} deg^{-2} except for the central G*G* residues in **III*** for which both hydrogen-bond-length and flat-angle restraints were reduced by one third, allowing for the more unusual base-pair geometry anticipated for these positions. Deoxyribose sugar puckers were deduced for sugar rings displaying clearly resolved H2′ and H2″ to H1′ DQF-COSY cross-peaks. The programs SPHINX and LINSHA[46] were used to perform simulations of DQF-COSY cross-peaks, by using a six component spin system (H1′, H2′, H2″, H3′, H4′ and P) with strong coupling only between geminal protons (H2′ and H2″). Coupling constants and resonance linewidths were systematically varied until the best match between simulated and experimental data was observed.[47]

Structure determination strategy: Canonical A- and B-DNA models were generated in Sybyl 6.3 by using the Tripos 5.4 force field.[48] DNA atom charges were calculated by using the Pullman method.[49] Backbone charges were reduced to incorporate counter-ion effects implicitly. The *cis*-diammineplatinum(II) residue was docked onto the N7 atoms of G7* and G8* after the first round of structure refinement for **III***. The bond lengths and angles for this fragment were set according to crystal structure data with the chloride ligands removed. Charges were assigned according to a reported molecular mechanics calculation.[14] Distance restraints from MARDIGRAS calculations were incorporated into A- and B-DNA starting models. For structure calculations of **III***, B-DNA starting models were subjected to 100 ps rMD simulations at 300 K during the first cycle of refinement. Force constants for the distance restraints were gradually increased from zero to a final maximum value of 20 kcal mol^{-1} Å^{-2} during the first few picoseconds of simulation. Initial velocities for rMD were assigned to a Boltzmann distribution. Coordinates of the final 5 ps of the dynamics trajectory were averaged. The resulting structure was energy-minimized to yield **III*B1**. The rMD calculations from A-DNA starting models were subjected to an initial forging phase during the first round of calculations. Over the first 31 ps the temperature was increased gradually from 0 to 900 K with a concomitant increase in the distance restraint force constant from 0 to 100 kcal mol^{-1} Å^{-2}. After 10 ps rMD at 900 K, the system was slowly cooled to 300 K over a 5 ps period when the force constant was simultaneously reduced to 20 kcal mol^{-1} Å^{-2}. The rMD simulations were continued at constant temperature to a total period of 100 ps. The final 5 ps were averaged and energy-minimized to yield **III*A1**. Structure calculations for **III** were carried out in a similar way, although by using shorter trajectory periods and a constant temperature of 300 K, to yield **IIIB1** and **IIIA1**. The structures **III*A1**, **III*B1**, **IIIA1**, and **IIIB1** were subsequently used as starting models in further MARDIGRAS calculations to yield new sets of distance restraints for a second round of rMD calculations. The structures were subjected to a series of shorter molecular-dynamics runs (20 ps each), the final 3 ps of which were averaged and energy-minimized to yield new starting structures **III*A2**, **III*B2**, **IIIA2**, and **IIIB2**. The final

  0947-6539/00/0619-3643 $ 17.50+.50/0

round of calculations resulted in a family of 10 converged structures for both **III** and **III***.

Structure analysis: The program CURVES 5.2[50] was used to analyze the resulting structures by using the helical parameters that describe a nucleic acid duplex: parameters were defined according to the EMBO workshop on DNA curvature and bending.[51]

Acknowledgement

This research was supported by the Biotechnology and Biological Sciences Research Council, Engineering and Physical Sciences Research Council (Biomolecular Sciences Programme), and the EC COST program. We are grateful to the Committee of Vice Chancellors and Principals of the Universities of the United Kingdom for an Overseas Research Student Award and the University of Edinburgh for a Research Studentship to Y. Chen. We thank the Wellcome Trust for funding molecular-modeling facilities, the Medical Research Council for magnet time at the National Institute of Medical Research, Mill Hill, and members of the COST D8 working group D8/009/97 for stimulating discussions.

Note added in proof: We thank L. G. Marzilli (Atlanta) and J. Kozelka (Paris) for recent stimulating discussions on our structures. The low intensity of the T6 H2′ DQF-COSY cross-peak of **III*** may be due to an N⇌S equilibrium for the T6 sugar ring. In the N conformer, the shielding of T6 H2′ by the G7* base more readily accounts for the observed chemical shift of the T6 H2′ resonance. Ring current shifts are potentially valuble aids for further refinement of the structure of the cross-linked region.[52]

[1] J. Reedijk, *J. Chem. Soc. Chem. Commun.* **1996**, 801 – 806.
[2] E. R. Jamieson, S. J. Lippard, *Chem. Rev.* **1999**, *99*, 2467 – 2498.
[3] E. Reed, R. F. Ozols, R. Tarone, S. H. Yuspa, M. C. Poirier, *Proc. Natl. Acad. Sci. USA* **1987**, *84*, 5024 – 5028.
[4] Y. Corda, M.-F. Anin, M. Leng, D. Job, *Biochemistry* **1992**, *31*, 1904 – 1908.
[5] L. J. N. Bradley, K. J. Yarema, S. J. Lippard, J. M. Essigmann, *Biochemistry* **1993**, *32*, 982 – 988.
[6] C. S. Chow, C. M. Barnes, S. J. Lippard, *Biochemistry* **1995**, *33*, 2954 – 2964.
[7] U. M. Ohndorf, J. P. Whitehead, N. L. Raju, S. J. Lippard, *Biochemistry* **1997**, *36*, 14807 – 14815.
[8] E. E. Trimmer, D. B. Zamble, S. J. Lippard, J. M. Essigmann, *Biochemistry* **1998**, *37*, 352 – 362.
[9] D. B. Zamble, D. Mu, J. T. Reardon, A. Sancar, S. J. Lippard, *Biochemistry* **1996**, *35*, 10004 – 10013.
[10] J.-C. Huang, D. B. Zamble, J. T. Reardon, S. J. Lippard, A. Sancar, *Proc. Natl. Acad. Sci. USA* **1994**, *91*, 10394 – 10398.
[11] S. E. Sherman, D. Gibson, A. H.-J. Wang, S. J. Lippard, *J. Am. Chem. Soc.* **1988**, *110*, 7368 – 7381.
[12] P. M. Takahara, C. A. Frederick, S. J. Lippard, *J. Am. Chem. Soc.* **1996**, *118*, 12309 – 12321.
[13] P. M. Takahara, A. C. Rosenzweig, C. A. Frederick, S. J. Lippard, *Nature* **1995**, *377*, 649 – 652.
[14] F. Herman, J. Kozelka, V. Stoven, E. Guittet, J.-P. Girault, T. Huynh-Dinh, J. Igolen, J.-Y. Lallemand, J.-C. Chottard, *Eur. J. Biochem.* **1990**, *194*, 119 – 133.
[15] D. Z. Yang, S. S. G. E. van Boom, J. Reedijk, J. H. van Boom, A. H.-J. Wang, *Biochemistry* **1995**, *34*, 12912 – 12920.
[16] A. Gelasco, S. J. Lippard, *Biochemistry* **1998**, *37*, 9230 – 9239.
[17] S. U. Dunham, S. U. Dunham, C. J. Turner, S. J. Lippard, *J. Am. Chem. Soc.* **1998**, *120*, 5395 – 5406.
[18] F. Reeder, Z. J. Guo, P. del Socorro Murdoch, A. Corazza, T. W. Hambley, S. J. Berners-Price, J.-C. Chottard, P. J. Sadler, *Eur. J. Biochem.* **1997**, *249*, 370 – 382.
[19] S. S. Wijmenga, M. M. W. Mooren, C. W. Hilbers in *NMR of Macromolecules, A Practical Approach* (Ed.: G. C. K. Roberts), Oxford University Press, New York, **1993**, pp. 217 – 288.
[20] K. Wüthrich, *NMR of Proteins and Nucleic Acids*, Wiley, New York, **1986**.
[21] J. A. Parkinson, S. E. Ebrahimi, J. H. McKie, K. T. Douglas, *Biochemistry* **1994**, *33*, 8442 – 8452.
[22] J. Kozelka, M.-H. Fouchet, J.-C. Chottard, *Eur. J. Biochem.* **1992**, *205*, 895 – 906.
[23] M.-H. Fouchet, E. Guittet, J. A. H. Cognet, J. Kozelka, C. Gauthier, M. Le Bret, K. Zimmermann, J.-C. Chottard, *J. Biol. Inorg. Chem.* **1997**, *2*, 83 – 92.
[24] S. Neidle, *DNA Structure and Recognition*, Oxford University Press, Oxford, **1994**.
[25] T. L. James in *An Encyclopedia of Nuclear Magnetic Resonance* (Eds.: D. M. Grant, R. K. Harris), Wiley, Chichester, **1996**, pp. 3330 – 3334.
[26] M. Tonelli, E. Ragg, A. M. Bianucci, K. Lesiak, T. L. James, *Biochemistry* **1998**, *37*, 11745 – 11761.
[27] S. J. Berners-Price, K. J. Barnham, U. Frey, P. J. Sadler, *Chem. Eur. J.* **1996**, *2*, 1283 – 1291.
[28] R. E. Dickerson, *Nucleic Acids Res.* **1998**, *26*, 1906 – 1926.
[29] V. Brabec, J. Reedijk, M. Leng, *Biochemistry* **1992**, *31*, 12397 – 12402.
[30] Y. Chen, J. A. Parkinson, Z. Guo, T. Brown, P. J. Sadler, *Angew. Chem.* **1999**, *111*, 2192 – 2196; *Angew. Chem. Int. Ed.* **1999**, *38*, 2060 – 2063.
[31] Y. Chen, Z. Guo, S. J. Parsons, P. J. Sadler, *Chem. Eur. J.* **1998**, *4*, 672 – 676.
[32] U.-M. Ohndorf, M. A. Rould, Q. He, C. O. Pabo, S. J. Lippard, *Nature* **1999**, *399*, 708 – 712.
[33] S. U. Dunham, S. J. Lippard, *Biochemistry* **1997**, *36*, 11428 – 11436.
[34] D. Locker, M. Decoville, J.-C. Maurizot, M. E. Bianchi, M. Leng, *J. Mol. Biol.* **1995**, *246*, 243 – 247.
[35] A. Schwartz, M. Leng, *J. Mol. Biol.* **1994**, *236*, 969 – 974.
[36] C. S. Chow, J. P. Whitehead, S. J. Lippard, *Biochemistry* **1994**, *33*, 15124 – 15130.
[37] A. Gelasco, S. J. Lippard in *Topics in Biological Inorganic Chemistry, Vol. 1* (Eds.: M. J. Clarke, P. J. Sadler), Springer, Berlin, **1999**, pp. 1 – 43.
[38] S. J. S. Kerrison, P. J. Sadler, *J. Chem. Soc. Chem. Commun.* **1977**, 861 – 864.
[39] S. J. Berners-Price, A. Corazza, Z. J. Guo, K. J. Barnham, P. J. Sadler, Y. Ohyama, M. Leng, D. Locker, *Eur. J. Biochem.* **1997**, *243*, 782 – 791.
[40] T.-L. Hwang, A. J. Shaka, *J. Magn. Reson. Ser. A* **1995**, *112*, 275 – 279.
[41] D. J. States, R. A. Haberkorn, D. J. Ruben, *J. Magn. Reson.* **1982**, *48*, 286 – 292.
[42] B. A. Borgias, T. L. James, *Methods Enzymol.* **1989**, *176*, 169 – 183.
[43] B. A. Borgias, T. L. James, *J. Magn. Reson.* **1990**, *87*, 475 – 487.
[44] K. Weisz, R. H. Shafer, W. Egan, T. L. James, *Biochemistry* **1994**, *33*, 354 – 366.
[45] W. Saenger, *Principles of Nucleic Acid Structure*, Springer, New York, **1984**.
[46] H. Widmer, K. Wüthrich, *J. Magn. Reson.* **1987**, *74*, 316 – 336.
[47] C. Gonzalez, W. Stec, A. Kobylanska, R. I. Hogrefe, M. Reynolds, T. L. James, *Biochemistry* **1994**, *33*, 11062 – 11072.
[48] M. Clark, R. D. Cramer, N. van Opdenbosch, *J. Comp. Chem.* **1989**, *10*, 982 – 1012.
[49] H. Berthod, A. Pullman, *J. Chim. Phys.* **1965**, *62*, 942 – 946.
[50] R. Lavery, H. Sklenar, *Curves 5.2: Helical Analysis of Irregular Nucleic Acids*, Laboratorie de Biochimie Theorique, Institut de Biologie Physico-Chimique, CNRS, Paris, France, **1997**.
[51] R. E. Dickerson, *J. Biomol. Struct. Dyn.* **1989**, *6*, 627 – 634.
[52] S. O. Ano, Z. Kuklenyik, L. G. Marzilli in *Cisplatin—Chemistry and Biochemistry of a Leading Anticancer Drug* (Ed.: B. Lippert), Wiley-VCH, Weinheim, **1999**, pp. 247 – 291.

Received: December 14, 1999 [F2190]

  0947-6539/00/0619-3644 $ 17.50+.50/0